ACCSCIENCE PUBLISHING

International Journal of Bioprinting

RESEARCH ARTICLE

Human airway-derived extracellular matrix bioinks for the engineering of proximal airway-like constructs: A proof-of-feasibility study

Heather Wanczyk[1], Nina D. Kosciuszek[1,2], Joanne Walker[1], Daniel J. Weiss[3]*, and Christine Finck[1,2]*

[1]Department of Pediatrics, University of Connecticut Health Center, Farmington, Connecticut, United States of America

[2]Department of Surgery, Connecticut Children's Medical Center, Hartford, Connecticut, United States of America

[3]Department of Medicine, Larner College of Medicine, University of Vermont, Burlington, Vermont, United States of America

Abstract

Three-dimensional bioprinting offers a promising strategy for the fabrication of physiologically relevant airway constructs; however, generating hollow, anatomically accurate proximal airway structures using tissue-specific bioinks with sufficient printability and mechanical stability remains challenging. This study describes the development and characterization of biocompatible, polymer-blended human airway-derived decellularized extracellular matrix (AW-dECM) bioinks for extrusion bioprinting of structurally and mechanically relevant proximal airway-like hollow constructs. A formulation consisting of 30 mg/mL AW-dECM and nanofibrillar cellulose–alginate conjugated to RGD supported the fabrication of simple and complex hollow airway structures with elastic moduli of approximately 8–10 kPa, within the range measured for bulk proximal airway tissue. The bioinks also supported preliminary primary human airway epithelial cell viability and adhesion, as well as gene expression patterns consistent with differentiation toward mucociliary and secretory phenotypes during the 28 days of air–liquid interface culture. Following subcutaneous implantation in immunocompetent rats, acellular AW-dECM polymer-blended bioinks maintained structural integrity over 30 days and were tolerated without evidence of infection or tissue necrosis, although a localized foreign body response was observed. Collectively, these findings demonstrate proof of concept for combining tissue-specific AW-dECM with commercially available printable polymers to fabricate mechanically relevant hollow airway-like constructs. This approach provides a basis for further development of advanced ex vivo airway models and regenerative airway engineering strategies.

Keywords: Airway-derived decellularized extracellular matrix; Three-dimensional bioprinting; Proximal airways; Polymer blended bioinks; Tissue engineering; Viscoelasticity

***Corresponding authors:**
Daniel J. Weiss (daniel.weiss@med.uvm.edu);
Christine Finck (Cfinck@connecticutchildrens.org)

Citation: Wanczyk H, Kosciuszek ND, Walker J, Weiss DJ, Finck C. Human airway-derived extracellular matrix bioinks for the engineering of proximal airway-like constructs: A proof-of-feasibility study. *Int J Bioprint*. 2026;12(5):026280295. doi: 10.36922/IJB026280295

Received: July 8, 2026

1st revised: August 2, 2026

2nd revised: August 8, 2026

Accepted: August 13, 2026

Published online: August 14, 2026

Copyright: © 2026 Author(s). This is an Open-Access article distributed under the terms of the Creative Commons Attribution License, permitting distribution, and reproduction in any medium, provided the original work is properly cited.

Publisher's Note: AccScience Publishing remains neutral with regard to jurisdictional claims in published maps and institutional affiliations.

1. Introduction

Ex vivo bioengineering approaches for proximal airways remain challenging despite

decades of research.[1-4] Emerging technologies such as three-dimensional (3D) bioprinting are now being applied to generate tracheal and airway constructs for congenital pediatric respiratory defects and for acute or chronic airway diseases or injury.[5-8] These scaffolds, combined with airway-specific stem cells, have the potential to regenerate airway epithelium and restore tissue structure following injury. As current treatments for congenital airway defects (i.e., laryngeal clefts,[9] tracheomalacia, bronchomalacia[10]) or respiratory diseases (i.e., cystic fibrosis[11] and primary ciliary dyskinesia[12]) fail to regenerate damaged or defective airway tissue, improved biofabrication strategies could significantly advance future therapeutic options.

An effective airway engineering strategy requires appropriate cell sources and biomaterials capable of supporting tissue organization while maintaining printability and structural fidelity. Previously used cell types for proximal airway modeling and engineering applications include human primary bronchial epithelial cells or induced pluripotent stem cells differentiated to basal epithelial progenitors that, when grown at an air–liquid interface, differentiate into a mature pseudostratified epithelium complete with functional mucociliary and secretory cells.[13-16] However, commonly used substrates such as polyethylene terephthalate membranes coated with purified extracellular matrix (ECM) proteins including collagen or Matrigel™ [17] fail to recapitulate the stiffness, viscoelasticity, and biochemical complexity of native airways. These limitations can alter cell morphology and transcriptional profiles, reducing the physiological relevance of engineered airway models. 3D bioprinting can overcome many of these limitations by enabling the fabrication of complex, physiologically relevant constructs that better mimic native airway mechanics and architecture while providing precise control over construct geometry.

Among candidate materials, ECM-derived materials are particularly promising because they contain a complex composition of structural proteins, glycoproteins, proteoglycans, and growth factors that regulate cell behavior and tissue homeostasis. Unlike biologically inert synthetic materials, ECM-derived materials can better support airway progenitor cell adhesion, growth, differentiation, and ongoing physiological remodeling, making them particularly attractive for pediatric tissue engineering applications. In several studies, decellularized ECM (dECM)-derived materials have enhanced the differentiation and function of seeded or embedded induced pluripotent stem cell-derived lung progenitors, primary airway, or alveolar epithelial cells.[18-21] To reduce immunogenicity, native tissues are processed using detergents such as sodium dodecyl sulfate or sodium deoxycholate that remove all cellular and antigenic components while preserving the ECM.[22] Compared with synthetic materials such as poly(lactic-co-glycolic) acid (PLGA) and polyethylene glycol, dECM retains tissue-specific biochemical constituents and mechanical properties that promote appropriate cell adhesion, proliferation, and differentiation. Additionally, dECM-derived materials have the potential to integrate with host tissue and undergo physiological remodeling over time,[23] which is important for pediatric patients whose airways continue to grow and develop.[24-27]

Despite these biological advantages, dECM exhibits low printability because of its inherently reduced mechanical strength.[28] Our recent work has demonstrated that human airway-derived dECM exhibits a low stiffness (~100–300 Pa),[29] making printed structures susceptible to gravity-induced deformation and limiting their ability to maintain complex geometries. Consequently, tissue-specific dECM is typically combined with mechanically supportive polymers such as alginate, gelatin, or synthetic materials including polycaprolactone or PLGA to provide structural support.[28] These blended formulations also increase shear-thinning behavior, a critical rheological property required for high-fidelity extrusion bioprinting.[30] In parallel, support bath technologies such as freeform reversible embedding of suspended hydrogels (FRESH) have enabled fabrication of complex hollow tissues by providing temporary mechanical support during printing. Using this approach, bioinks are extruded into gelatin microparticle support baths containing ionic crosslinking agents that facilitate gelation and stabilize intricate 3D architectures.[31]

In the present study, we developed and characterized the suitability of regionally isolated human airway-derived dECM (AW-dECM) blended with alginate and nanofibrillar cellulose-RGD (Cellink-RGD) bioinks for extrusion bioprinting of hollow proximal airway-like constructs. AW-dECM–Cellink-RGD bioinks exhibited rheological and mechanical properties suitable for extrusion bioprinting, with elastic moduli within the range measured for native proximal airway tissue (~10–20 kPa)[32] and supported the fabrication of simplified and anatomically relevant hollow airway-like constructs with sufficient printability and shape fidelity. Primary human airway epithelial cells seeded on the bioinks remained viable and differentiated toward mucociliary and secretory phenotypes over 28 days of air–liquid interface culture. Following subcutaneous implantation in rats, bioinks maintained structural integrity over 30 days and were generally well tolerated despite a localized foreign body response (FBR). Collectively, these findings demonstrate the feasibility of integrating tissue-specific AW-dECM

with printable polymer blends to fabricate hollow airway-like constructs with biologically and mechanically relevant characteristics. This work provides a foundation for the continued development of physiologically relevant *ex vivo* airway models and future airway biofabrication strategies.

2. Materials and methods

2.1. Human lung decellularization and airway-specific isolation

Human lungs from normal, healthy patients (2 donors) with no known lung diseases or smoking history were obtained from the Autopsy Services at the University of Vermont, under appropriate institutional guidelines and Health Insurance Portability and Accountability Act protections, and were decellularized using established protocols.[33,34] Adequacy of decellularization was demonstrated by a lack of intact cells or cell debris on hematoxylin and eosin (H&E)-stained, mounted 5 μm paraformaldehyde-fixed sections, no intact bands on DNA gels, and <50 ng DNA/ug protein.[33,34] Airway-specific regions were then isolated from decellularized lungs using a previous protocol.[34] To produce the hydrogel, airway preparations were cryomilled, lyophilized, and digested under constant mixing over 72 h using 1 mg/mL pepsin (Thermo Fisher Scientific, USA) + 0.01 M hydrochloric acid (Thermo Fisher Scientific, USA).[34,35] Insoluble aggregates were removed by centrifuging the mixture at 600 rpm for 20 mins. The resulting supernatant containing the digested lung tissue was removed, transferred to a new conical tube, and pH-balanced to 7.0 by adding 1:9 (v/v) 0.1 M sodium hydroxide. Samples were then frozen at −80 °C for 24 h and lyophilized for an additional 72 h. The decellularized lung tissues and subsequent hydrogel preparations used in this study have previously been extensively characterized for protein and glycosaminoglycan contents.[29,33]

2.2. Preparation of airway-derived decellularized extracellular matrix polymer-blended bioinks for mechanical studies

Polymer-blended AW-dECM bioinks (30 mg/mL) were prepared by solubilizing 45 mg lyophilized airway tissue in 1.5 mL Cellink-RGD bioinks (Cellink, Sweden). Briefly, lyophilized lung tissue was added to a 3 mL syringe and mixed with Cellink-RGD. The bioink suspension was mixed using two 3 mL syringes connected via a female-female luer lock until a homogeneous solution was obtained. Solubilized bioinks were then placed on ice for at least 1 h. For comparison, 45 mg lyophilized AW-dECM was also resuspended in 1.5 mL cold Dulbecco's Modified Eagle Medium (Thermo Fisher Scientific, USA) and placed on ice for solubilization over 1 h.

2.3. Preparation of airway-derived decellularized extracellular matrix polymer-blended bioinks for three-dimensional bioprinting studies

Polymer-blended AW-dECM bioinks (30 mg/mL) were prepared by solubilizing 90 mg lyophilized decellularized airway tissue in 3 mL Cellink-RGD bioinks (Cellink, Sweden). Samples were mixed using two 3 mL syringes connected via a female-female luer lock until a homogeneous solution was obtained. The solubilized bioinks were then placed on ice for at least 1 h before printing, then loaded into a 3 mL gas-tight Hamilton syringe.

2.4. Oscillatory rheology measurements of airway-derived decellularized extracellular matrix Cellink-RGD bioinks

To assess the mechanical properties of 30 mg/mL AW-dECM alone and 30 mg/mL AW-dECM combined with Cellink-RGD bioink, a DHR-3 Discovery Rheometer (TA Instruments, USA) was utilized. A total volume of 600 μL of each crosslinked, previously swollen phosphate-buffered saline (PBS) hydrogel sample (n = 6 per hydrogel type) was loaded onto a 12 mm parallel steel plate pre-warmed to 37 °C. Gap height was set to 1,000 μm with 1% strain and 0.159 Hz frequency (1.0 rad/s). Oscillatory frequency sweeps were performed at 37 °C on all materials, and the storage modulus (G') and loss modulus (G") were determined. To assess the shear-thinning behavior (printability) or viscosity of AW-dECM–Cellink-RGD bioinks, flow sweep tests were performed on uncrosslinked samples (n = 6) using a 12 mm parallel steel plate set to 25 °C, gap height = 1,200 μm, and shear rate = 0.001/s to 200/s.

2.5. Scanning electron microscopy analysis of bioink preparations

A total concentration of 30 mg/mL AW-dECM alone or blended with Cellink-RGD bioink (n = 3 per bioink type) was prepared for scanning electron microscopy (SEM) analysis. Briefly, 30 mg/mL AW-dECM–Cellink-RGD was prepared as above and crosslinked with 0.1% $CaCl_2$ for 1.5 h, then rinsed with 1 × PBS and incubated at 37 °C for 1 h. Moreover, 30 mg/mL AW-dECM alone was placed in a 3D-printed polylactic acid (PLA)-based Transwell (Matter Hackers, USA) (8 mm × 2 mm). Samples were then crosslinked for 1 hr at 37 °C and subsequently fixed with 2.5% glutaraldehyde in 0.1 M cacodylate buffer at room temperature for an additional 1 h. For post-fixation steps, samples were submerged in 1% osmium tetroxide and 0.8% ferricyanide in 0.1 M cacodylate buffer at room temperature for 1 h. Samples were then rinsed three times with 0.1 M cacodylate buffer, followed by rinsing with

distilled water (three times). Samples were dehydrated with ethanol for over 40 mins and dried using a 1:2 solution of hexamethyldisilazane and 100% ethanol, followed by a 2:1 solution of hexamethyldisilazane and ethanol for 20 mins each. For the final steps, samples were rinsed in 100% hexamethyldisilazane for 20 mins (twice). Samples were then sputter-coated with gold and imaged using a JEOL JSM-5900LV (Japan) SEM.

2.6. Fabrication of a three-dimensional bioprinter from a commercially available fused deposition modeling printer

The material used for bioprinting is listed in Table S1. A Flash Forge Adventurer 5M desktop printer (Flashforge, China) was modified into a 3D bioprinter based on a concept developed by researchers at Carnegie Mellon[36] (Figure S1). Briefly, computer-aided design (CAD) files were uploaded and 3D-printed to assemble the syringe pump (Replistruder) required for layer-by-layer deposition of bioinks (Figure S1A). The original parts were removed from the printer, and the 3D-printed Replistruder parts were assembled (Figure S1B and S1C). Next, the original Wi-Fi board was removed and replaced with a Duet Wi-Fi board following a previous protocol[36] (Figure S1D).

2.7. Conversion of pediatric airway computed tomography scan into a three-dimensional printable file

Using an open-source online medical data repository (embodi3D), a computed tomography scan of a pediatric airway was acquired, and corresponding DICOM files were uploaded into the imaging platform Slicer 4.11. No Health Insurance Portability and Accountability Act-protected information was obtained or utilized for the scan. Files were converted into .stl files and modified in SolidWorks (version 2019). The converted airway model was then uploaded into PRUSA software (version 2.9.5), whereby it was modified and converted into G-code for subsequent bioprinting (Figure S2). The final dimensions were 65 mm × 60 mm × 27 mm with 100% rectilinear infill.

2.8. Freeform reversible embedding of suspended hydrogel support preparation

Freeform reversible embedding of suspended hydrogels v2.0 gelatin microparticle support bath solutions were prepared using a complex coacervation method based on a previous protocol.[37] Briefly, 125 mL of distilled water was added to a 500 mL glass beaker and heated to 50 °C, followed by the addition of 125 mL of 100% ethanol (Thermo Fisher Scientific, USA). The solution was then treated with 3% gelatin B (Thermo Fisher Scientific, USA), 0.3% gum arabic, and 0.125% Pluronic, added stepwise. A stir bar was placed in the solution, and the beaker was covered with parafilm, followed by stirring at 350 rpm overnight. The following day, stirring was stopped to allow the formed gelatin microparticles to settle. After approximately 30 mins, the excess ethanol was removed. Gelatin microparticles were collected in a 50 mL conical tube and centrifuged at 750× *g* for 3 mins. The excess solution was decanted, followed by rinsing, mixing the samples with distilled water, and spinning at 1,000× *g* for 3 mins (twice). For the final step, the support bath was mixed with 0.1% $CaCl_2$, spun at 1,000× *g* for 3 mins, and then set aside for subsequent printing. All support bath materials were used within a 2-h period to prevent material dehydration.

2.9. Extrusion-based three-dimensional bioprinting of patient-specific airway and simplified hollow airway structure

Simplified hollow airway structures (50 mm × 40 mm × 20 mm) were created using SolidWorks. Additionally, hollow cylinders (20 mm × 10 mm × 2 mm and 20 mm × 5 mm × 1 mm) were designed using Tinkercad (https://www.tinkercad.com/). 3D models were uploaded into PRUSA and converted into G-code reflecting the diameter of the syringe and needle used for bioprinting. These files were then uploaded into the custom-built bioprinter. All prints were constructed using a 30-G needle (inner diameter: 0.160 mm, outer diameter: 0.310 mm) (Jensen Global, USA), with a layer height of 0.06 mm and 3 perimeters. For the support bath setup, FRESH slurry was added to a 100 mm tissue culture dish and prepared for bioprinting. Prepared bioinks were placed into a 3 mL Hamilton gas-tight syringe and loaded into the Replistruder syringe pump for FRESH bioprinting. Following extrusion of inks within the gelatin microparticle support bath containing the 0.1% $CaCl_2$ crosslinker, the airway scaffolds were released by incubating the print containers at 37 °C for 1.5 h and rinsing with 1× PBS.

2.10. Culture and seeding of primary human airway epithelial stem cells on three-dimensional bioprinted airway-derived decellularized extracellular matrix–Cellink-RGD bioinks

Lung tissues for primary human airway epithelial cell isolation (one donor) were deidentified and obtained from the University of Iowa Cells and Tissues Core in the Precision Medicine Center for Cystic Fibrosis with approval of the University of Iowa Institutional Review Board (ID #: 199507432). Isolated primary human airway epithelial cells derived from these tissues and used in this study were graciously provided by the Ryan Lab at the University of Iowa State. A total of 500,000 cells were cultured and

expanded in T75 flasks (Thermo Fisher Scientific, USA) using PneumaCult-Ex Medium (STEMCELL Technologies, Canada) supplemented with A0830-01 (Fisher Scientific, USA), DMH1 (Sigma Aldrich, USA), hydrocortisone (Stemcell Technologies, USA), and Rho-associated protein kinase inhibitor (Tocris Bioscience, USA). Airway cells (P2) were seeded at 50,000 cells/disc (6 mm × 1 mm thick), crosslinked for 1.5 h in 0.1% $CaCl_2$, rinsed twice with PBS, and incubated at 37 °C for 1 h in Transwell inserts, then cultured in Pneumacult-EX medium for four days. Cells were then airlifted, and differentiation medium (PneumaCult™ ALI Medium; STEMCELL Technologies, Canada) supplemented with hydrocortisone and heparin was added to the basal compartment of the wells (n = 16). The experiment was replicated twice to confirm reproducibility. Cells were then harvested on Day 28 for quantitative polymerase chain reaction (qPCR) analysis.

2.11. *In vitro* assessment of airway epithelial cell viability on three-dimensional bioprinted airway-derived decellularized extracellular matrix–Cellink-RGD bioinks

To assess the biocompatibility of airway cells seeded on 30 mg/mL AW-dECM–Cellink-RGD bioinks, samples from above were incubated with a Live/Dead assay using calcein acetoxymethyl ester/ethidium bromide staining (Thermo Fisher Scientific, USA) at 37 °C for 10 mins on Days 1, 3, 7, and 14 (n = 3/day). Briefly, 5 µL of calcein acetoxymethyl ester and 2.5 µL of ethidium bromide were added to 5 mL of 1× PBS and mixed thoroughly. The staining solution was then added to the samples, which were incubated at 37 °C for 10 min and subsequently imaged by fluorescence microscopy. Samples were evaluated using a Zeiss LSM 880 (Germany) microscope. The experiment was replicated twice to confirm reproducibility of findings.

2.12. Quantitative polymerase chain reaction analysis of airway cells seeded on three-dimensional bioprinted airway-derived decellularized extracellular matrix–Cellink-RGD bioinks

On Day 28, airway cells seeded on bioinks (n = 4 constructs, biological replicates = 2) were treated with 1 mL Trizol/well per manufacturer's protocol (Thermofisher Scientific, USA). Following cell lysis, 200 µL chloroform was added to each sample, vortexed, and incubated at room temperature for 2–3 mins. Samples were then centrifuged at 12,000× g for 15 mins at 4 °C. Following centrifugation, the top phase was removed, and 500 µL of isopropanol was added and mixed. Samples were incubated at room temperature for 10 mins and then centrifuged as above for an additional 10 mins to precipitate the isolated RNA. Following centrifugation, the supernatant was removed, and 350 µL RLT lysis buffer was added to the RNA pellet. A total volume of 350 µL of 70% ethanol was added to the sample, mixed, and dispensed into a column for RNA purification (74104, RNeasy Minikit, Qiagen, the Netherlands). RNA concentration was determined using a NanoDrop spectrometer (Thermo Fisher Scientific, USA). Housekeeping genes *B2M* and *YWHAZ* were used for normalization of gene expression. The list of genes and primers used is given in Table S2.

2.13. Subcutaneous implantation of acellular three-dimensional bioprinted airway-derived decellularized extracellular matrix–Cellink-RGD bioinks in rats

To assess biocompatibility and degradation of bioinks, bioprinted samples (Cellink-RGD alone[control] or 30 mg/mL AW-dECM–Cellink-RGD [treatment]; 8 mm × 3 mm discs) were implanted subcutaneously (control: left side, treatment: right side) in the lateral dorsal region of Sprague–Dawley rats, weighing 300–500 g (16 weeks of age, n = 24; 14 females, 10 males; Charles River Laboratories, USA). All animal work was previously approved by the University of Connecticut Health Institutional Animal Care and Use Committee (Protocol #: AP-210081-1126). No randomization or predefined exclusion criteria were applied. Males and females were divided equally among the different groups. Before surgery, rats were kept in a temperature-controlled environment (22 °C) with 50% relative humidity and a 12-hour light/12-hour dark cycle, with access to water and food as needed. Anesthesia was administered using 4% isoflurane via a nose cone. Two 3-cm incisions were made, one on the left side and one on the right side of the lateral dorsum in each rat under sterile conditions. Each animal received one sample of Cellink-RGD bioink and one sample of 30 mg/mL AW-dECM–Cellink-RGD bioink circular discs. Bioinks were implanted in a subcutaneous pocket between the skin and muscle of each rat and closed with 3-0 Vicryl suture. Post-operatively, all animals received ketoprofen (Zoetis, USA) subcutaneously once daily for three days for pain management. On Days 3, 14, and 30, eight rats per time point were euthanized via CO_2 overdose to evaluate biocompatibility (fibrosis, inflammation, and presence of granulation tissue), angiogenesis, and degradation. Four animals from the Day 30 group were used for mechanical and degradation assessments of the implanted constructs, while the remaining four animals were used to evaluate cellular infiltration and fibrosis.

2.14. Histological analysis

Tissue samples were fixed in 10% formalin (Thermo Fisher Scientific, USA) for 24 h. Samples were then embedded in paraffin, and 5 µm or 10 µm sections were cut using a

microtome. For histological assessments, samples were mounted on positively charged slides (Thermo Fisher Scientific, USA) and stained with H&E (NC1470670, Fisher Scientific, USA) and Masson's trichrome (87019, Thermo Scientific, USA) stain to evaluate cellular infiltration/fibrosis. Investigator blinding was performed for all microscopy image analyses. Six fields per scaffold were scanned, and quantitative analysis of cellular infiltration (6 images/sample, 10 measurements/image) was performed using ImageJ software (version 1.54p).

2.15. Immunofluorescence staining

For immunofluorescence staining, tissue sections were blocked and permeabilized for 45 min in staining solution containing 1× PBS, 0.2% Tween 20 (Fisher Scientific, USA), 5% fetal bovine serum (Gibco/Fisher Scientific, USA), and 0.2% Triton X-100 (Fisher Scientific, USA). Primary antibodies against CD163 (1:100; BS-2527R, Thermo Fisher Scientific, USA), inducible nitric oxide synthase (iNOS; 1:100; PA1-036, Thermo Fisher Scientific, USA), and myeloperoxidase (1:100; PA5-16672, Thermo Fisher Scientific, USA) were diluted in the staining solution, and sections were incubated overnight at 4 °C. The following day, sections were washed twice with PBS for 2 min each and incubated with goat anti-rabbit Alexa Fluor 488 secondary antibody (1:200; A-11008; Thermo Fisher Scientific, USA) for 1 h at room temperature in the dark. Sections were subsequently washed twice with PBS for 2 min each and counterstained with DAPI (1:100) in 1 × PBS for 10 min at room temperature in the dark. After two additional washes with 1 × PBS, sections were mounted using Immu-Mount (9990402, Fisher Scientific, USA) and imaged by fluorescence microscopy.

2.16. Statistical analysis

For analysis of capsule thickness/cellular infiltrate using H&E, measurements obtained from multiple images within each implant were averaged to generate one value per implant. Because each animal received one Cellink-RGD implant and one AW-dECM–Cellink-RGD implant, material measurements were treated as paired observations within each animal. Different groups of animals were euthanized at each implantation time point; therefore, material was analyzed as a within-animal repeated factor and implantation time as a between-animal factor. Data were analyzed using a two-way analysis of variance, and Šídák's multiple-comparisons test was used to compare materials within each time point. The animal was considered the biological experimental unit.

Statistical significance of the qPCR data obtained from airway cells seeded on 30 mg/mL AW-dECM compared to 30 mg/mL AW-dECM–alginate-RGD blended bioinks was assessed using one-way analysis of variance with Tukey's multiple comparisons (GraphPad Prism; version 11). Housekeeping genes used for normalization were *YWHAZ* and *B2M*. Statistical significance was determined at $^{*}p < 0.05$, $^{**}p < 0.01$, $^{***}p < 0.001$, and $^{****}p < 0.0001$ ($n = 4$ technical replicates, $N = 2$ biological replicates: study repeated twice using the same donor cells). Data were calculated using the $2^{-\Delta\Delta Ct}$ method, and statistical analysis was performed on fold-change gene expression values.

3. Results

3.1. Enhanced mechanical properties of airway-derived decellularized extracellular matrix polymer-blended RGD bioinks

The topography and mechanical properties of 30 mg/mL AW-dECM–Cellink-RGD bioink samples were assessed using SEM and oscillatory rheometry (Figure 1). Analysis of bioink topography using SEM showed that AW-dECM–Cellink-RGD bioinks had a smooth and less porous surface compared to 30 mg/mL AW-dECM alone (Figure 1A and B). Collagen fibers were evident in both samples (Figure 1B). Flow sweeps performed on AW-dECM–Cellink-RGD bioinks demonstrated excellent shear-thinning behavior as indicated by a decrease in viscosity with increasing shear rate (~15 kPa·s at 0.01/s compared to ~1.0 Pa·s at 200/s) (Figure 1C). Frequency sweeps also revealed that both materials exhibited viscoelastic properties: 30 mg/mL AW-dECM–Cellink-RGD and Cellink-RGD alone exhibited a statistically significantly higher storage modulus (~8 kPa) compared to 30 mg/mL AW-dECM alone (~100 Pa) (Figure 1D and E).

3.2. Successful bioprinting of simplified and computed tomography-derived hollow airway structures using airway-derived decellularized extracellular matrix polymer-blended bioinks

To assess the printability and shape fidelity of 30 mg/mL AW-dECM–Cellink-RGD bioinks, hollow cylinders (10 mm diameter × 2 mm height × 2 mm wall thickness) were bioprinted using the FRESH approach. After preparing the gelatin microparticle slurry bath (Figure 2A–D), extrusion multiplier rate settings ranging from 0.55–1.3 were modified using PrusaSlicer 2.8.0 software prior to printing to determine the optimal rate for filament integrity and strength. Five hollow cylinders, each bioprinted using a different multiplier rate, were extruded into FRESH support baths and removed by placing the printed cylinders at 37 °C for 1.5 h (Figure 2E). Based on subsequent print height, rate of bioink shrinkage after two hours at room temperature, and structural integrity as verified by bright-

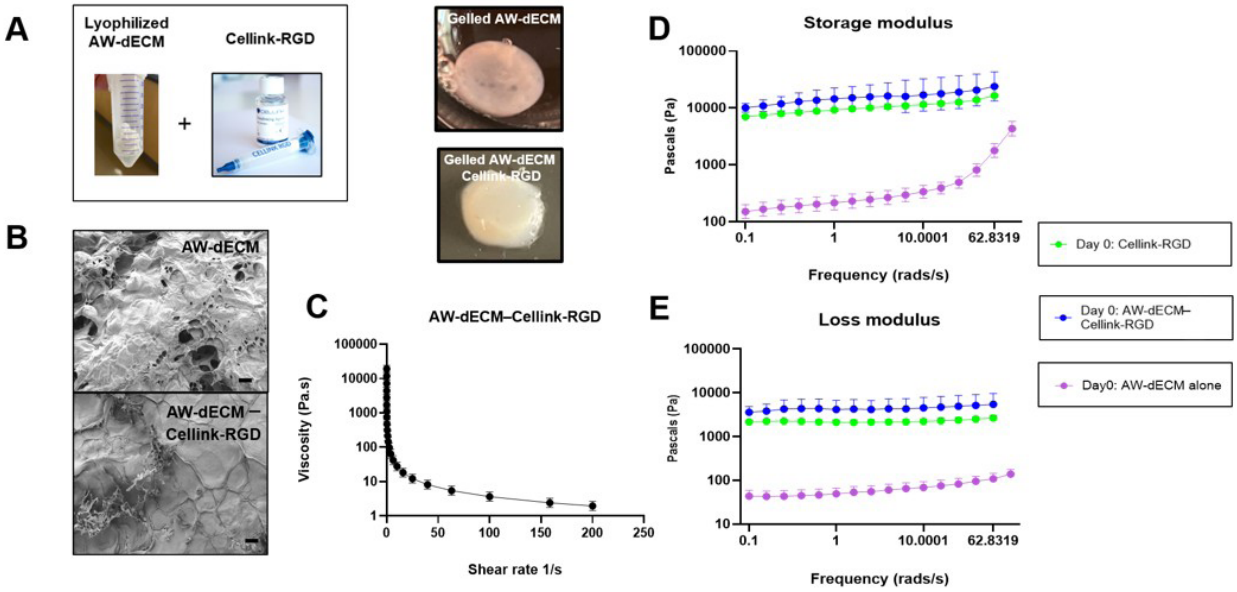


Figure 1. Mechanical and physical characterization of airway-derived decellularized extracellular matrix (AW-dECM)–Cellink-RGD bioinks. (A) Macroscopic images of gelled AW-dECM alone and gelled AW-dECM–Cellink-RGD prior to scanning electron microscopy (SEM) analysis. (B) SEM images of AW-dECM vs. AW-dECM–Cellink-RGD. Scale bars: 200 μm; magnification: 5×. Black arrows indicate the presence of collagen fibers. (C) Flow sweep evaluating viscosity of AW-dECM–Cellink-RGD bioinks in Pa.s (n = 6). (D, E) Frequency sweep evaluating storage and loss modulus (Pa) of AW-dECM alone vs. Cellink-RGD alone vs. AW-dECM–Cellink-RGD. Data represented as mean ± standard deviation; n = 6 per material type tested.

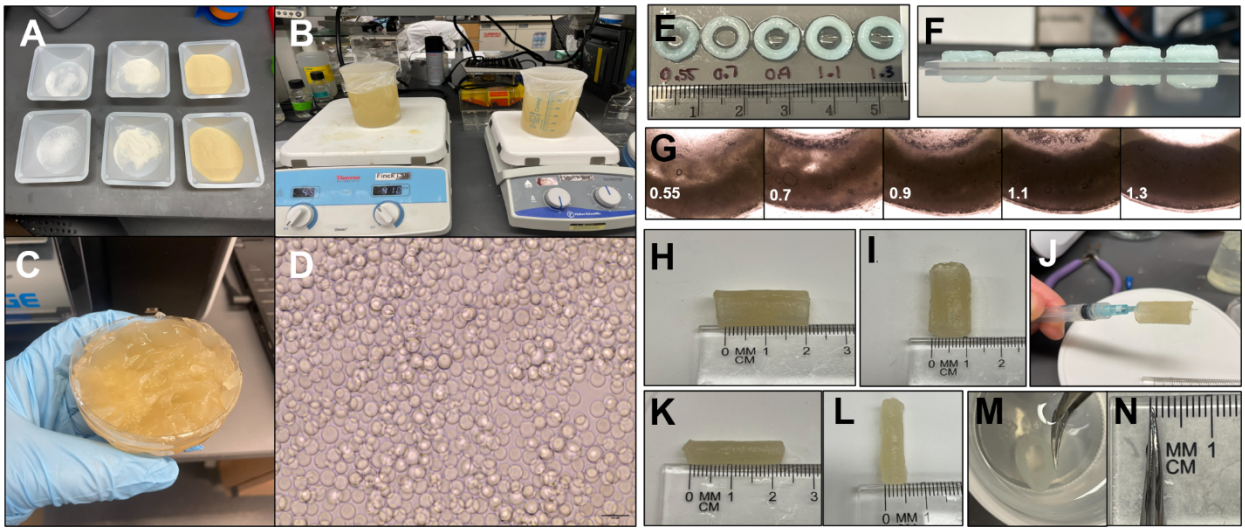


Figure 2. Freeform reversible embedding of suspended hydrogels (FRESH) support preparation and proof of concept for three-dimensional bioprinting hollow cylinders using airway-derived decellularized extracellular matrix (AW-dECM) polymer-blended bioink. (A–D) Preparation of FRESH support and bright-field image of uniform gelatin microparticles. Scale bar: 50 μm; magnification: 20×. (E, F) Testing of different extrusion flow rates for optimal filament density and construct height/thickness. (G) Bright-field images of hollow cylinders bioprinted using different extrusion flow rates. (H–J) Hollow cylinder measuring 20 mm × 10 mm × 2 mm bioprinted using the FRESH approach + 30 mg/mL AW-dECM–Cellink-RGD bioink. (K, L) Hollow cylinder measuring 20 mm × 5 mm × 1 mm, bioprinted using the FRESH approach + 30 mg/mL AW-dECM–Cellink-RGD bioink. (M, N) Wall thickness of bioprinted cylinder (20 mm × 5 mm × 1 mm) in mm.

field microscopy, it was determined that an extrusion multiplier rate of 1.3 resulted in the most mechanically stable filament structure (Figure 2E–G). Using these settings, hollow cylinders representing the thickness of a child's upper airway (20 mm × 5 mm × 1 mm and 20 mm × 10 mm × 2 mm in size) were successfully bioprinted and removed from the bath following incubation at 37 °C for 1.5 h. Measurements of the cylinders' diameter and length confirmed that they matched the dimensions of the original CAD files and could be manipulated without collapsing (Figure 2H–L). Measurements of the cylinders shown in Figure 2K and L showed a wall thickness of 1 mm (Figure 2M and N). Next, we evaluated the ability to bioprint more complex hollow airway structures using AW-dECM–Cellink-RGD bioinks (Figure 3A), which included two simplified hollow airway structures (Figure 3B and C) and a computed tomography-derived pediatric airway construct (Figure 3D). Each bioprinted airway construct was successfully printed a total of three times (quantitative measurements of wall thickness were not taken at this time). For each construct, the intended hollow geometries were accurately bioprinted with high fidelity and resolution into FRESH support baths using a 30-G needle and rectilinear infill pattern set at 100%. Following printing, the airway constructs were successfully removed by incubating the bath at 37 °C for 1.5 h.

3.3. Enhanced viability, adhesion, and spreading of primary airway epithelial cells on airway-derived decellularized extracellular matrix Cellink-RGD bioinks *in vitro*

To assess *in vitro* biocompatibility, Cellink bioinks conjugated with RGD peptides were combined with 30 mg/mL AW-dECM, as described previously. Human primary airway epithelial cells successfully adhered to bioinks and exhibited excellent spreading and viability by Day 3 (Figure 4A). Additionally, growth and spreading further increased by Day 14, as indicated by calcein acetoxymethyl ester/ethidium bromide staining, demonstrating the *in vitro* cytocompatibility of these bioinks with primary human airway epithelial stem cells (Figure 4A).

3.4. Differentiation of seeded human airway epithelial cells into mucociliary and secretory phenotypes over 28 days on RGD-conjugated airway-derived decellularized extracellular matrix polymer-blended bioinks

Quantitative PCR analysis revealed the differentiation

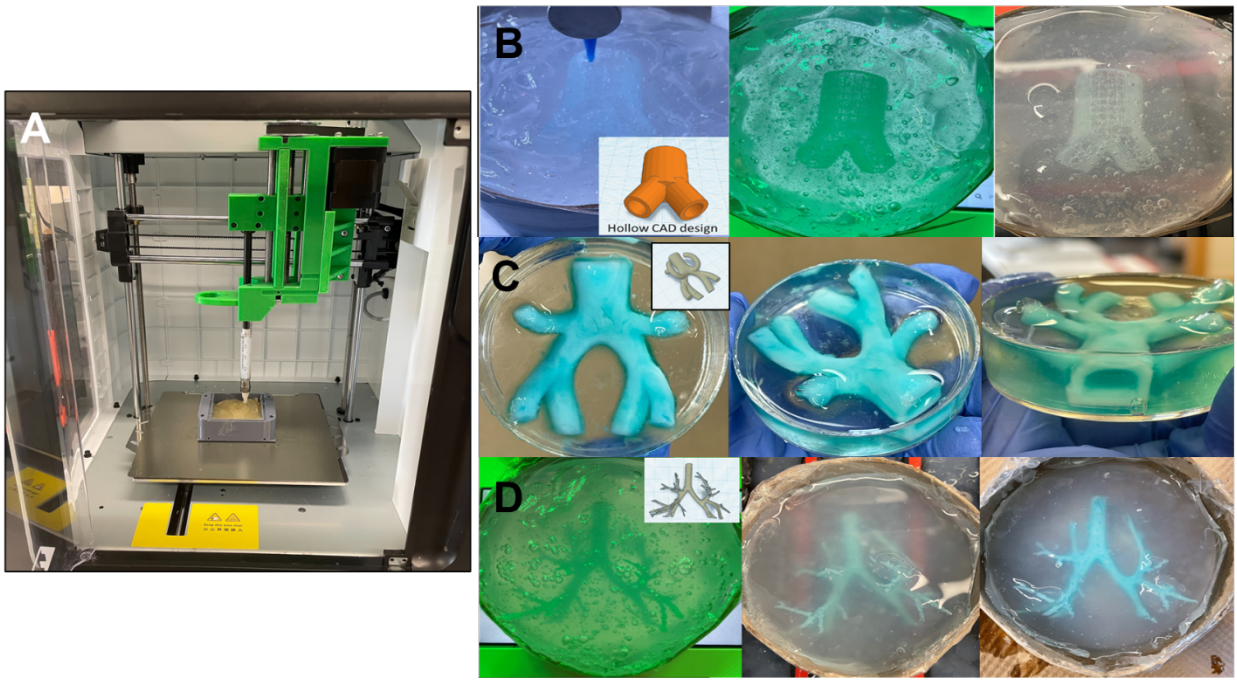


Figure 3. Simplified and computed tomography-derived hollow airway structures three-dimensionally (3D) bioprinted using airway-derived decellularized extracellular matrix (AW-dECM)–Cellink-RGD bioink and the freeform reversible embedding of suspended hydrogels approach. (A) Image of FlashForge Adventurer 3D printer converted into a 3D bioprinter. (B) 3D bioprinted airway-like structure printed into a support bath. (C) 3D bioprinted simplified, hollow airway structure. Blue food dye added for visualization. (3D) 3D bioprinted airway structure derived from a pediatric computed tomography scan. Blue food dye added for visualization.

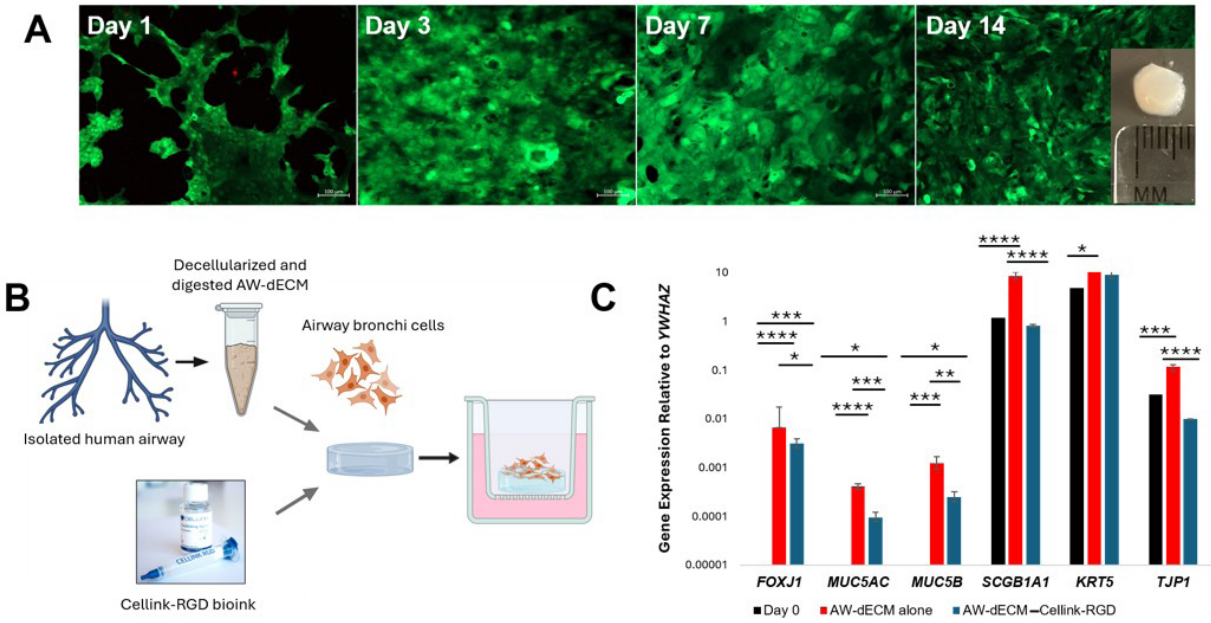


Figure 4. Viability and characterization of primary human airway epithelial cells seeded on airway-derived decellularized extracellular matrix (AW-dECM)–Cellink-RGD bioinks cultured at air–liquid interface over 28 days. (A) Live/Dead analysis of primary human airway epithelial cells seeded on top of 30 mg/mL AW-dECM–Cellink-RGD bioink over 14 days. Scale bar: 100 μm; magnification: 10×. (B) Schematic of cell seeding experiment. (C) Quantitative polymerase chain reaction analysis of *FOXJ1, MUC5AC, MUC5B, SCGB1A1, KRT5*, and *TJP1* expression in primary human airway epithelial cells (P2) seeded on 30 mg/mL AW-dECM–Cellink-RGD bioinks. Data presented as mean ± standard deviation. Statistical significance determined at $*p < 0.05$, $**p < 0.01$, $***p < 0.001$, and $****p < 0.0001$; $n = 4$ technical replicates, $N = 2$ biological replicates (two independent experiments).

of primary human airway cells seeded on bioinks to mucociliary and secretory phenotypes over 28 days (Figure 4B and C). Results were compared to Day 0 cells and airway cells seeded on 30 mg/mL AW-dECM alone for 28 days. Results revealed a statistically significant increase in *FOXJ1* expression in primary airway cells seeded on AW-dECM alone and AW-dECM–Cellink-RGD compared to Day 0 ($p \leq 0.0001$ and $p \leq 0.001$, respectively) (Figure 4C). There was also a statistically significant increase in *MUC5AC* and *MUC5B* expression across both conditions compared to Day 0. For *MUC5AC* expression, there was a statistically significant increase in AW-dECM–Cellink-RGD vs. Day 0 samples ($p \leq 0.05$) and AW-dECM alone vs. Day 0 samples ($p \leq 0.0001$) (Figure 4C). For *MUC5B* expression, there was a statistically significant increase in AW-dECM–Cellink-RGD vs. Day 0 samples ($p \leq 0.05$) and AW-dECM alone vs. Day 0 samples ($p \leq 0.001$) (Figure 4C). In terms of *SCGB1A1* expression, there was no significant difference in Day 0 vs. AW-dECM–Cellink-RGD samples; however, there was a statistically significant increase in samples seeded on AW-dECM alone vs. Day 0 and AW-dECM–Cellink-RGD ($p \leq 0.0001$) (Figure 4C). There was also a statistically significant increase in basal cell expression (*KRT5*) in cells seeded on AW-dECM alone compared to Day 0 samples ($p \leq 0.05$); however, no difference in expression was observed between cells at Day 0 and cells seeded on AW-dECM–Cellink-RGD, indicating basal cell phenotype was maintained over the 28-day period (Figure 4C). Overall, *TJP1* expression was elevated on AW-dECM alone compared to Day 0 and AW-dECM–Cellink-RGD samples.

3.5. Limited degradation and biocompatibility of acellular airway-derived decellularized extracellular matrix–Cellink-RGD bioinks following one-month subcutaneous implantation in a rat model

Sprague–Dawley rats implanted with bioprinted Cellink-RGD and AW-dECM–Cellink-RGD bioink samples over 30 days demonstrated excellent health with no signs of swelling or surgical site infection. Following tissue harvest on Days 3, 14, and 30, macroscopic evaluation of harvested implantation sites revealed no signs of necrosis, edema, infection, or tissue rejection (Figure S3A–G). On Day 3, Cellink-RGD bioink samples were largely mobile within the skin, indicating a lack of encapsulation within the subcutaneous wall and muscle layer. AW-dECM–Cellink-RGD bioinks were immobile on Day 3, and gross macroscopic evaluation of harvested implantation sites revealed the presence of a pocket-shaped hole within the subcutaneous wall where the bioinks were deposited

(Figure S3G). By Days 14 and 30, both bioink types were encapsulated within the tissue, as indicated by a lack of mobility within the skin. At the microscopic level, H&E staining of both bioink types at all time points showed no tissue integration (Figure 5); however, cellular infiltration was evident at the bioink–tissue interface (Figure S4). Measurement of this layer at Days 14 and 30 in animals implanted with both Cellink-RGD and AW-dECM–Cellink-RGD bioinks revealed no significant differences in thickness between the two samples in each animal and at both time points (Figure S4B).

Masson's trichrome staining demonstrated the presence of a typical FBR, evident by the formation of a fibrotic capsule surrounding the implanted bioink (Figure 6).

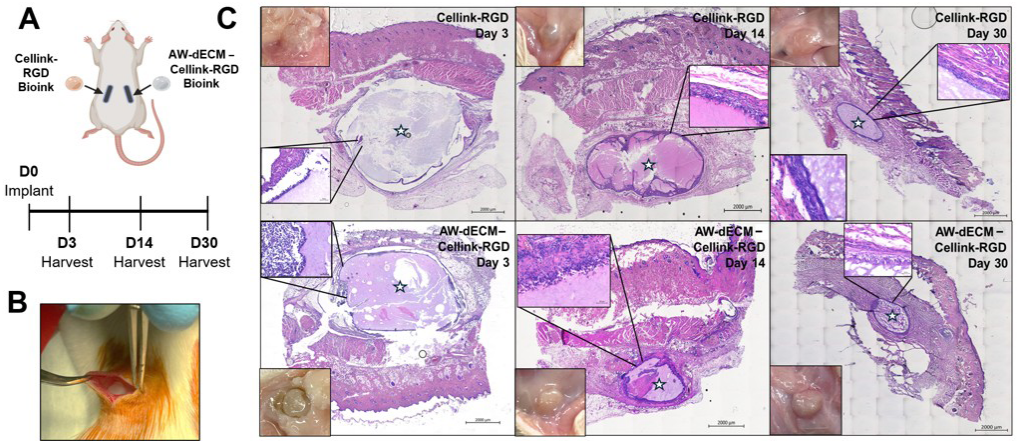


Figure 5. Representative hematoxylin and eosin staining of acellular Cellink-RGD and airway-derived decellularized extracellular matrix (AW-dECM)–Cellink-RGD bioinks implanted subcutaneously in immunocompetent Sprague–Dawley rats over 30 days. (A) Outline of experimental approach and timeline (n = 8 rats/time point harvested). Images are representative paired observations from one animal per time point. (B) Imaging depicting placement of bioink into subcutaneous tissue pocket. (C) Representative hematoxylin and eosin staining of implanted bioinks at different time points. A white star symbol denotes subcutaneously implanted bioink. Scale bars: 1,000 μm, 2,000 μm; magnifications: 5×. Inset hematoxylin and eosin images of the bioink edge: 50 μm; magnification: 20×. Inset macroscopic images in the upper left (top panels) and lower left (bottom panels) depict bioink following tissue harvest at Day 3, Day 14, and Day 30.

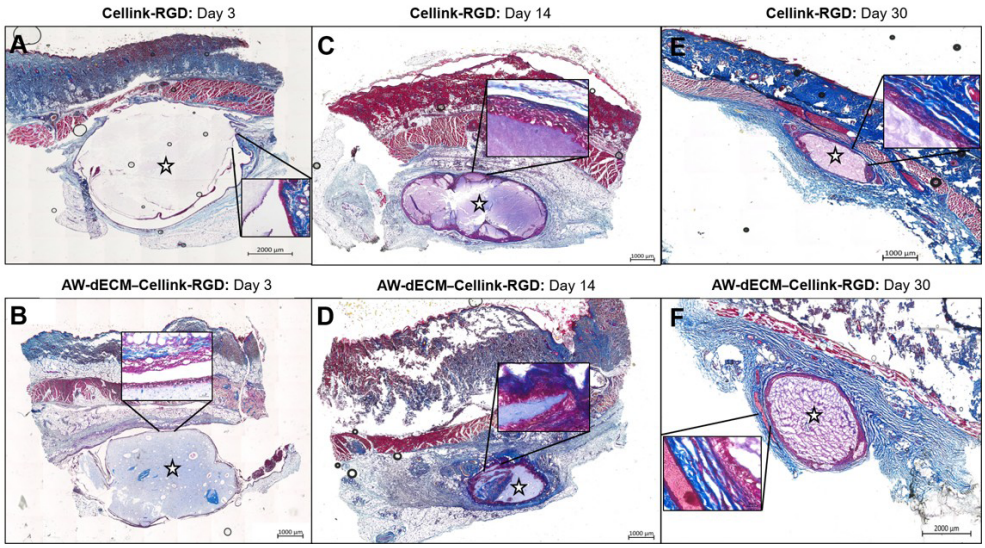


Figure 6. Representative Masson's trichrome staining of acellular Cellink-RGD and airway-derived decellularized extracellular matrix (AW-dECM)–Cellink-RGD bioinks implanted subcutaneously in immunocompetent Sprague–Dawley rats over 30 days. (A, B) Cellink-RGD and AW-dECM–Cellink-RGD on Day 3. (C, D) Cellink-RGD and AW-dECM–Cellink-RGD on Day 14. (E, F) Cellink-RGD and AW-dECM–Cellink-RGD on Day 30. The star symbols denote subcutaneously implanted bioinks. Scale bars: 1,000 μm, 2,000 μm; magnification: 5×. Inset images: scale bar: 50 μm; magnification: 20×.

Immunofluorescence staining of Day 3 bioink samples with a neutrophil-specific marker, myeloperoxidase, confirmed the presence of acute inflammatory cells on the bioink surface and in the surrounding tissues following bioink implantation (Figure S5), which resolved by Day 14 (Figure S6). Additionally, immunofluorescent staining with CD163$^+$ and iNOS$^+$ antibodies suggested the presence of M1 and M2 macrophage cell populations in proximity to the bioink at Days 14 and 30 (Figure 7). Prior to mechanical evaluation of Day 30 implanted

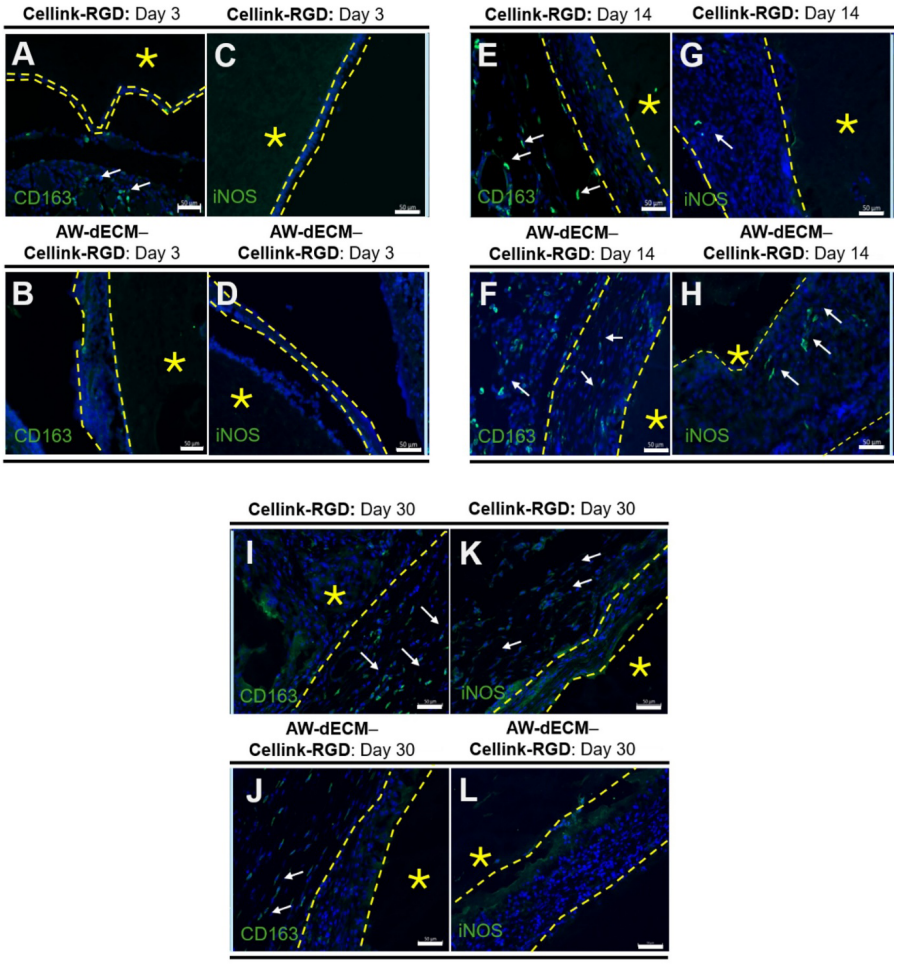


Figure 7. Representative immunofluorescent analysis of cell populations present at the bioink–tissue interface at Days 3, 14, and 30. (A, B) CD163$^+$ staining of cells at the bioink–tissue interface in Cellink-RGD and airway-derived decellularized extracellular matrix (AW-dECM)–Cellink-RGD samples on Day 3. (C, D) iNOS$^+$ staining of cells at the bioink–tissue interface in Cellink-RGD and AW-dECM–Cellink-RGD samples on Day 3. (E, F) CD163$^+$ staining of cells at the bioink–tissue interface in Cellink-RGD and AW-dECM–Cellink-RGD samples on Day 14. (G, H) iNOS$^+$ staining of cells at the bioink–tissue interface in Cellink-RGD and AW-dECM–Cellink-RGD samples on Day 14. (I, J) CD163$^+$ staining of cells at the bioink–tissue interface in Cellink-RGD and AW-dECM–Cellink-RGD samples on Day 30. (K, L) iNOS$^+$ staining of cells at the bioink–tissue interface in Cellink-RGD and AW-dECM–Cellink-RGD samples on Day 30. Yellow dotted lines demarcate the bioink–tissue interface; the yellow star denotes the bioink sample. White arrows indicate cells with positive staining. Scale bar: 50 μm; magnification: 20×.

bioinks, fibrous tissue encapsulated around the structures was removed to allow for accurate assessment of potential degradation (biological replicates = 4, technical replicates = 3). Comparison of the storage and loss moduli of Day 0 vs. Day 30 bioinks showed no significant difference between Cellink-RGD alone and AW-dECM–Cellink-RGD, suggesting minimal degradation over the 30-day period following transplantation (Figure 8A and B). To further support this assessment, Day 30 bioinks showed no change in diameter compared with Day 0 for either bioink (Figure 8C and D).

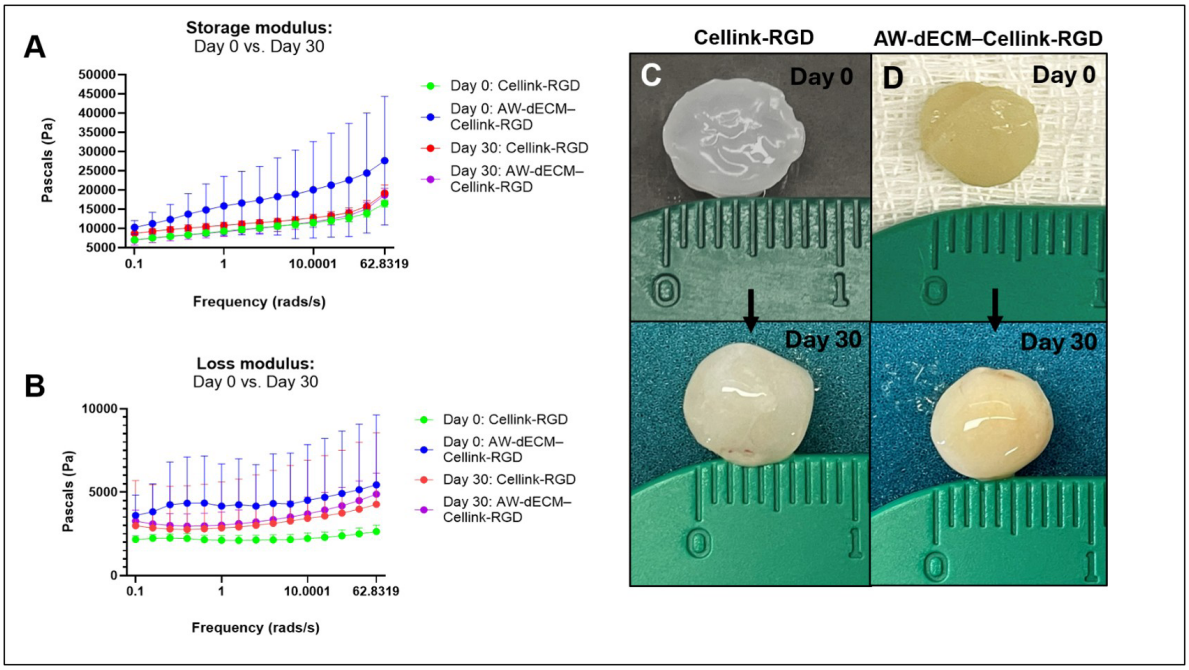


Figure 8. Mechanical assessment and structural evaluation of Cellink-RGD and airway-derived decellularized extracellular matrix (AW-dECM)–Cellink-RGD bioinks following subcutaneous implantation in rats over 30 days. (A) Storage modulus in Pa (frequency sweep) of Cellink-RGD vs. AW-dECM–Cellink-RGD bioinks at Day 0 vs. Day 30 of subcutaneous implantation. (B) Loss modulus in Pa (frequency sweep) of Cellink-RGD vs. AW-dECM–Cellink-RGD bioinks at Day 0 vs. Day 30 of subcutaneous implantation. Data represented as mean ± standard deviation; $n = 6$ bioinks/time point (Day 0), $n = 4$ bioinks/time point (Day 30). (C, D) Measurement of Cellink-RGD and AW-dECM–Cellink-RGD bioinks at Day 0 vs. Day 30.

4. Discussion

Despite significant advances in airway engineering, biofabrication of physiologically relevant proximal airway constructs remains challenging because current approaches often cannot simultaneously recapitulate tissue-specific biochemical composition, mechanical properties, sufficient printability, and anatomically relevant hollow architectures. Here, we developed and characterized a human AW-dECM-based polymer-blended bioink that combines tissue-specific ECM components with polymer-enhanced printability and structural stability. This biofabrication strategy enabled the successful fabrication of both simplified hollow airway structures and anatomically relevant airway-like constructs generated from computed tomography scans while exhibiting bulk mechanical properties within the range measured for native airway tissue. Primary human airway epithelial cells seeded on the bioinks and cultured at an air–liquid interface for 28 days remained viable, adhered, and spread across the constructs, and exhibited gene expression patterns consistent with differentiation toward mucociliary and secretory phenotypes. *In vivo* studies in immunocompetent rats showed that acellular bioinks were tolerated without infection or tissue necrosis over 30 days, although a typical FBR developed after implantation. Collectively, these findings demonstrate the feasibility of incorporating tissue-specific ECM into polymer-blended bioinks for proximal airway biofabrication.

The present findings also highlight several limitations that remain in proximal airway engineering. While past studies have demonstrated successful bioprinting of airway-like constructs, many have relied on purified ECM proteins or synthetic biomaterials that prioritize printability over biological complexity.[38,39] Conversely, tissue-specific dECM materials often provide a more physiologically relevant microenvironment but lack the mechanical properties needed to fabricate stable hollow structures. This limitation is due, in part, to the decellularization and bioink formation process, during which pepsin digestion disrupts collagen telopeptides and reduces the mechanical stability of the resulting biomaterial.[40] This often renders the material too soft for extrusion-based bioprinting, limiting its ability to maintain shape following deposition into a support bath or culture dish. The addition of natural or synthetic polymers substantially enhances the mechanical properties of dECM bioinks, improving printability and shape fidelity. In the present study, commercially available alginate conjugated to RGD was selected as the polymer component because

it is naturally derived, inexpensive, and demonstrates enhanced biocompatibility, cell adhesion, and printability compared to alginate alone and other synthetic bioinks such as polyethylene glycol and PLGA.[41]

By combining airway-specific dECM with a mechanically supportive polymer blend, the present approach addresses the limited mechanical stability of dECM while retaining tissue-specific biochemical cues important for airway engineering. Our previous characterization of the AW-dECM used in this study demonstrated that it is highly enriched in collagen I, VI, laminin, fibronectin, and other cartilaginous collagens, all of which are important ECM proteins involved in cell attachment, growth, and differentiation.[29] Consistent with these findings, other studies have demonstrated that tissue-specific bioinks more closely recapitulate the native tissue microenvironment because of their inherent biochemical composition, making them attractive for clinically relevant tissue engineering applications and drug-screening platforms.[42-46] Likewise, our previous work also demonstrated that AW-dECM is biocompatible and supports mucociliary and secretory differentiation of primary human bronchial epithelial cells,[29] providing the rationale for incorporating AW-dECM into the polymer-blended bioinks evaluated in the present study. Although researchers have investigated tissue-specific dECM bioinks across several organ systems, few studies have evaluated human AW-dECM combined with printable polymer blends to fabricate hollow airway constructs. Consequently, the present work extends previous studies by incorporating regionally isolated human AW-dECM into a mechanically reinforced bioink and evaluating its printability, epithelial cell compatibility, and *in vivo* host response.

Compared to AW-dECM alone, AW-dECM blended with Cellink-RGD exhibited enhanced mechanical properties that substantially improved structural fidelity, enabling the development of stable hollow airway constructs. The storage moduli (~8–10 kPa) of the polymer-blended bioinks more closely reflect average bulk mechanical values reported for native proximal airway tissue (~10–20 kPa) compared to AW-dECM alone (~100 Pa), enabling the successful bioprinting of hollow airway-like structures with improved shape fidelity.[47] In addition to elastic modulus, shear-thinning behavior is an important determinant of extrusion bioprinting performance because it permits bioinks to flow under shear while rapidly recovering viscosity following deposition.[48] This characteristic enabled the AW-dECM–Cellink-RGD formulation to generate stable hollow geometries using the FRESH approach. While the current study focused primarily on bulk mechanical characterization, native proximal airway tissue is mechanically heterogeneous.[49] Therefore, future studies should evaluate regional mechanical heterogeneity throughout printed constructs and its influence on airway cell behavior. Incorporating chondrocytes and stromal cell populations into 3D bioprinted airway constructs may also better mimic the mechanical properties found across different regions of the upper airways.

Based on our *in vitro* findings, gene markers associated with mucociliary and secretory differentiation were elevated in airway epithelial cells seeded on AW-dECM–Cellink-RGD bioinks, though at lower levels than in AW-dECM alone. Despite this, epithelial cells remained viable and differentiated toward both ciliated and secretory phenotypes, suggesting that incorporating Cellink-RGD did not eliminate the instructive effects of airway-derived ECM but may have altered the efficiency of epithelial differentiation. This may be due to differences in cell–matrix interactions associated with the polymer blend, including reduced matrix remodeling resulting from the lower degradability of alginate, altered ligand presentation, or other changes in the biochemical and mechanical environment.[50] Future studies should investigate the effects of Cellink-RGD alone to determine its full contributions to airway epithelial differentiation.

Overall, similar tradeoffs between printability and biological activity have been reported for numerous polymer-blended dECM bioinks.[51] Because these mechanisms were not directly evaluated in the present study, additional work is needed to determine their relative contributions. Furthermore, protein-level characterization and morphological analyses using multiple epithelial cell donors will also be necessary to confirm successful epithelial differentiation and function. Nevertheless, the present findings demonstrate that polymer-blended AW-dECM bioinks support preliminary airway epithelial cell viability and growth while providing the mechanical properties required for extrusion bioprinting, highlighting their potential for future airway biofabrication applications.

Our *in vivo* results showed that subcutaneously implanted bioinks were tolerated without evidence of necrosis or infection in immunocompetent Sprague–Dawley rats over 30 days. After 30 days, the bioinks maintained their original size and bulk mechanical properties as indicated by macroscopic and rheological evaluation of harvested bioinks at Day 0 and Day 30. However, a typical FBR to both Cellink-RGD alone and AW-dECM–Cellink-RGD bioinks was evident by Days 14 and 30. Histological staining revealed a well-formed fibrous capsule in both conditions by the end of one month. Development of a fibrous capsule following implantation

is a common outcome for implanted biomaterials and does not necessarily indicate material failure.[52] Rather, the extent of this response can be influenced by several factors including biomaterial composition, degradation rate, surface characteristics, and mechanical properties.[53] Overall, these findings are consistent with previous reports describing host responses to implanted hydrogel-based biomaterials.[23,54-56] Additionally, limited data currently exist related to the *in vivo* host response to alginate-RGD biomaterials, as most studies primarily focus on their *in vitro* performance.[57-59] Therefore, the present study extends characterization of this airway bioprinting approach by providing information on the *in vivo* host response to commercially available alginate-RGD biomaterials following implantation in immunocompetent animals. To reduce the severity of the FBR, pre-clinical studies have suggested incorporating anti-inflammatory bioactive peptides or cytokines, such as interleukin-4, into biomaterials to promote macrophage polarization toward M2 phenotypes.[60-62] In the present study, assessment of the cell types within the fibrous capsule at Day 30 suggested the presence of both M2 and M1 macrophages, as indicated by $CD163^+$ and $iNOS^+$ staining. This is consistent with previous studies demonstrating the important role of macrophages in regulating the FBR to implanted hydrogels.[63] The mixed M1/M2 macrophage phenotype observed in this study may reflect distinct immunogenic signals from the Cellink-RGD bioink and tissue-specific dECM components, with alginate potentially contributing to the FBR,[64] while AW-dECM may provide immunomodulatory cues that influence macrophage polarization.[65,66] However, as the thickness of the cell infiltrate/fibrotic capsule did not differ between Cellink-RGD and AW-dECM–Cellink-RGD implants, the contribution of AW-dECM to this response may be negligible. Currently, there is no standard for predicting the immunogenicity of tissue-specific dECM; therefore, studies evaluating residual MHC and antigen glycan content, cryptic particle abundance, and ECM structural alterations following processing will help elucidate its full contribution to the FBR response.[67] These findings will also help guide future modifications to bioink composition to promote a more favorable host immune response.

Future studies could evaluate incorporating anti-inflammatory components into AW-dECM–Cellink-RGD bioinks to determine whether host response and integration can be improved. In addition to biochemical modification of the bioink, modulating its mechanical properties may offer another strategy to influence the host immune response following implantation. One study showed that stiffer hydrogels (~10 kPa) promoted a more pro-inflammatory macrophage phenotype than softer hydrogels (<2 kPa).[68] Therefore, future studies could investigate modulation of bioink stiffness, for example through reduced crosslinking time, to determine whether a slightly softer substrate promotes a more favorable host immune response while maintaining sufficient structural integrity for airway biofabrication.

Another study also investigated the utility of alginate-blended (without RGD) bulk lung bioinks for 3D bioprinting lung-specific tissue. Researchers found that the material exhibited excellent printability and biocompatibility for embedded and seeded primary human epithelial cells; however, the samples were subcutaneously implanted in a mouse model of transplant immunosuppression.[69] By comparison, the present study evaluated Cellink-RGD and AW-dECM–Cellink-RGD bioinks in immunocompetent hosts, providing complementary information regarding the host response when the innate immune system remains intact. Although these materials have demonstrated favorable *in vitro* cytocompatibility, the present findings indicate that they remain susceptible to a typical FBR following implantation. These observations highlight the importance of evaluating both *in vitro* performance and *in vivo* host responses when developing biomaterials intended for regenerative applications.

Another aspect that will require further investigation is the degradation rate of the bioink. Controlled degradation represents an important design consideration because airway replacements must initially withstand repetitive respiratory forces while eventually permitting replacement by host-derived tissue.[70] Consequently, the degradation rate must provide sufficient structural support during the early stages of implantation while allowing cellular infiltration and matrix remodeling over time. For load-bearing tubular tissues such as the airway, premature degradation could compromise lumen patency and mechanical integrity, whereas excessively slow degradation may delay host integration and adaptive remodeling. Therefore, an intermediate degradation profile that provides initial structural support while permitting gradual host-mediated remodeling and vascularization is most desirable.[71] In the present study, AW-dECM–Cellink-RGD bioinks remained structurally intact following 30 days of subcutaneous implantation, suggesting that substantial degradation had not yet occurred. However, longer-term implantation studies (6 months to 1 year) are needed to determine whether the degradation profile is appropriate for future airway applications. If the bioinks persist *in vivo*, one strategy would be to incorporate matrix metalloproteinase-sensitive peptides to promote controlled matrix degradation. In one study, incorporation of matrix metalloproteinase-2-sensitive peptides into

alginate hydrogels laden with human mesenchymal stem cells increased material degradation and improved tissue integration following subcutaneous implantation in xenograft mouse models.[72]

Limitations of this study include the use of xenogeneic materials to assess host immune response and overall biocompatibility, as well as evaluation of acellular constructs rather than cell-laden implants. Future studies using decellularized rat airway tissue combined with Cellink-RGD will determine whether host response and tissue integration improve in immunocompetent animals. While the subcutaneous implantation model provides valuable information regarding biocompatibility and host response, it cannot fully replicate the biomechanical loading, airflow, mucosal environment, or microbial exposure encountered within the native airway. Consequently, interpretation of these findings should be limited to assessment of material compatibility rather than prediction of orthotopic airway performance. Therefore, the host response and structural integrity of bioprinted airways following orthotopic implantation will need to be evaluated, as the airway represents a substantially different mechanical and immunological environment. To address this, future studies should develop a small-animal airway defect model to iteratively evaluate these responses and further assess the translational potential of AW-dECM–Cellink-RGD bioinks. Future studies should also quantitatively validate print fidelity and reproducibility, including comparisons between CAD designs and printed constructs (wall thickness measurements) and assessment of inter-print variability.

5. Conclusion

In conclusion, this study demonstrates the feasibility of a human airway-like biofabrication approach for producing mechanically stable hollow airway constructs using polymer-blended AW-dECM bioinks. Through characterization of rheological behavior, mechanical properties, printability, preliminary epithelial cell compatibility, and *in vivo* host response, these findings demonstrate that tissue-specific AW-dECM can be successfully integrated with commercially available printable polymers to fabricate hollow airway constructs possessing structural and mechanical characteristics relevant to proximal airway tissue. Although further optimization of immune compatibility, matrix remodeling, and orthotopic implantation will be required before clinical translation, this work provides a foundation for continued development of physiologically relevant *ex vivo* airway models and future tissue-engineered airway replacements.

Acknowledgments

We acknowledge the generous donation of human primary airway cells from the Ryan Lab at the University of Iowa, which were used in this study.

Funding

Research reported in this publication was supported by the National Institute of Arthritis and Musculoskeletal and Skin Diseases of the National Institutes of Health (Award Number T32AR079114 and R21 HD104069, NSF Recode 3 Award 2225554). The content is solely the responsibility of the authors and does not necessarily represent the official views of the National Institutes of Health.

Conflict of interest

The authors declared no potential conflicts of interest with respect to the research, authorship, and/or publication of this article.

Author contributions

Conceptualization: Heather Wanczyk, Daniel J. Weiss, Christine Finck
Data curation: Heather Wanczyk, Joanne Walker
Formal analysis: Heather Wanczyk
Funding acquisition: Daniel J. Weiss, Christine Finck
Investigation: All authors
Methodology: Heather Wanczyk, Daniel J. Weiss, Christine Finck
Project administration: Daniel J. Weiss, Christine Finck
Supervision: Daniel J. Weiss, Christine Finck
Writing–review & editing: All authors
Writing–original draft: Heather Wanczyk

Ethics approval and consent to participate

All animal work was approved by the Institutional Animal Care and Use Committee at the University of Connecticut Health Center (Protocol #: AP-210081-1126). Deidentified human lungs were obtained from the University of Vermont (UVM) autopsy services. Ethical clearance was not required for use of the materials. Per UVM policy, research involving deceased people is not considered human subject research and does not require IRB review. Deidentified lung tissues for human bronchial epithelial cell (HBEC) isolation were obtained from donor lungs from the University of Iowa Cells and Tissues core in the Precision Medicine Center for Cystic Fibrosis with approval of the University of Iowa Institutional Review Board (ID #: 199507432). Primary human bronchial epithelial cells were provided through the Cells, Tissues and Models core funded by NIH-NIDDK P30 DK054759-22 (to ALR).

Consent for publication

Not applicable.

Availability of data

Data are available from the corresponding authors upon reasonable request.

Further disclosure

This paper has been uploaded to or deposited as a preprint on bioRxiv (doi: 10.64898/2026.06.04.730194).

References

1. Atale N, Ling Z, Ren X, *et al*. Establishing an Ex Vivo Culture Model of Human Proximal Airway Tissue. *Methods Protoc*. 2025;8(6):20251102.

   doi: 10.3390/mps8060132

2. Heise RL. Computational, Ex Vivo, and Tissue Engineering Techniques for Modeling Large Airways. *Adv Exp Med Biol*. 2023;1413:107-120.

   doi: 10.1007/978-3-031-26625-6_6

3. Lee-Ferris RE, Okuda K, Galiger JR, *et al*. Prolonged airway explant culture enables study of health, disease, and viral pathogenesis. *Sci Adv*. 2025;11(17):eadp0451.

   doi: 10.1126/sciadv.adp0451

4. Han JJ. Surgeon who implanted the world's first artificial trachea found guilty of causing bodily harm. *Artif Organs*. 2022;46(9):1720-1721.

   doi: 10.1111/aor.14358

5. Zhang Y, Liu Y, Shu C, *et al*. 3D bioprinting of the airways and lungs for applications in tissue engineering and in vitro models. *J Tissue Eng*. 2024;15:20417314241309183.

   doi: 10.1177/20417314241309183

6. Park JH, Ahn M, Park SH, *et al*. 3D bioprinting of a trachea-mimetic cellular construct of a clinically relevant size. *Biomaterials*. 2021;279:121246.

   doi: 10.1016/j.biomaterials.2021.121246

7. Bae SW, Lee KW, Park JH, *et al*. 3D Bioprinted Artificial Trachea with Epithelial Cells and Chondrogenic-Differentiated Bone Marrow-Derived Mesenchymal Stem Cells. *Int J Mol Sci*. 2018;19(6):1624.

   doi: 10.3390/ijms19061624

8. Torsello M, Salvati A, Borro L, *et al*. 3D bioprinting in airway reconstructive surgery: A pilot study. *Int J Pediatr Otorhinolaryngol*. 2022;161:111253.

   doi: 10.1016/j.ijporl.2022.111253

9. Johnston DR, Watters K, Ferrari LR, *et al*. Laryngeal cleft: evaluation and management. *Int J Pediatr Otorhinolaryngol*. 2014;78(6):905–911.

   doi: 10.1016/j.ijporl.2014.03.015

10. Hysinger EB. Laryngomalacia, Tracheomalacia and Bronchomalacia. *Curr Probl Pediatr Adolesc Health Care*. 2018;48(4):113-118.

    doi: 10.1016/j.cppeds.2018.03.002

11. Shteinberg M, Haq IJ, Polineni D, *et al*. Cystic fibrosis. *Lancet*. 2021;397(10290):2195-2211.

    doi: 10.1016/s0140-6736(20)32542-3

12. Despotes KA, Zariwala MA, Davis SD, *et al*. Primary Ciliary Dyskinesia: A Clinical Review. *Cells*. 2024;13(12):974.

    doi: 10.3390/cells13110974

13. Myo YPA, Camus SV, Freeberg MAT, *et al*. Protocol for differentiating primary human small airway epithelial cells at the air-liquid interface. *Am J Physiol Lung Cell Mol Physiol*. 2025;328(6):L757-l771.

    doi: 10.1152/ajplung.00380.2024

14. Berical A, Beermann ML, Suzuki S, *et al*. Generation of Airway Epithelial Cell Air-Liquid Interface Cultures from Human Pluripotent Stem Cells. *J Vis Exp*. 2022(184):e63882.

    doi: 10.3791/63882

15. Chen L, Gabriela AH, Pathinayake PS, *et al*. Inflammation-induced loss of CFTR-expressing airway ionocytes in non-eosinophilic asthma. *Respirology*. 2025;30(1):25-40.

    doi: 10.1111/resp.14833

16. Moses E, Wang T, Corbett S, *et al*. Molecular Impact of Electronic Cigarette Aerosol Exposure in Human Bronchial Epithelium. *Toxicol Sci*. 2017;155(1):248-257.

    doi: 10.1093/toxsci/kfw198

17. Brocke SA, Speen AM, Masood S, *et al*. Comparison of permeable cell culture inserts for use in culture of a human in vitro air–liquid interface model system. *Physiol Rep*. 2024;12(3):e15921.

    doi: 10.14814/phy2.15921

18. Hoffman ET, Uriarte JJ, Uhl FE, *et al*. Human alveolar hydrogels promote morphological and transcriptional differentiation in iPSC-derived alveolar type 2 epithelial cells. *Sci Rep*. 2023;13(1):12057.

    doi: 10.1038/s41598-023-37685-x

19. Noori A, Mokhber Dezfouli MR, Rajabi S, *et al*. Decellularized lung extracellular matrix scaffold promotes human embryonic stem cell differentiation towards alveolar progenitors. *Cell J*. 2023;25(6):372-382.

    doi: 10.22074/cellj.2023.563370.1148

20. Garlíková Z, Silva AC, Rabata A, *et al*. Generation of a Close-to-Native In Vitro System to Study Lung Cells-Extracellular Matrix Crosstalk. *Tissue Eng Part C Methods*. 2018;24(1):1-13.

doi: 10.1089/ten.tec.2017.0283

21. Gilpin SE, Ren X, Okamoto T, *et al*. Enhanced lung epithelial specification of human induced pluripotent stem cells on decellularized lung matrix. *Ann Thorac Surg*. 2014;98(5):1721-1729.

doi: 10.1016/j.athoracsur.2014.05.080

22. Ohata K, Ott HC. Human-scale lung regeneration based on decellularized matrix scaffolds as a biologic platform. *Surg Today*. 2020;50(7):633-643.

doi: 10.1007/s00595-020-02000-y

23. Aamodt JM, Grainger DW. Extracellular matrix-based biomaterial scaffolds and the host response. *Biomaterials*. 2016;86:68-82.

doi: 10.1016/j.biomaterials.2016.02.003

24. Elomaa L, Almalla A, Keshi E, *et al*. Rise of tissue- and species-specific 3D bioprinting based on decellularized extracellular matrix-derived bioinks and bioresins. *Biomater Biosyst*. 2023;12:100084.

doi: 10.1016/j.bbiosy.2023.100084

25. Liu H, Gong Y, Zhang K, *et al*. Recent Advances in Decellularized Matrix-Derived Materials for Bioink and 3D Bioprinting. *Gels*. 2023;9(3):195.

doi: 10.3390/gels9030195

26. Yu C, Ma X, Zhu W, *et al*. Scanningless and continuous 3D bioprinting of human tissues with decellularized extracellular matrix. *Biomaterials*. 2019;194:1-13.

doi: 10.1016/j.biomaterials.2018.12.009

27. Lian L, Xie M, Luo Z, *et al*. Rapid Volumetric Bioprinting of Decellularized Extracellular Matrix Bioinks. *Adv Mater*. 2024;36(34): e2304846.

doi: 10.1002/adma.202304846

28. Zhang H, Wang Y, Zheng Z, *et al*. Strategies for improving the 3D printability of decellularized extracellular matrix bioink. *Theranostics*. 2023;13(8):2562-2587.

doi: 10.7150/thno.81785

29. Wanczyk H, Porritt L, Linke J, *et al*. Characterization of human airway-derived decellularized extracellular matrix hydrogels and their effects on airway epithelial cell growth, organization and differentiation. *Biomaterials*. 2027;336:124420.

doi: 10.1016/j.biomaterials.2026.124420

30. Cai Y, Chang SY, Gan SW, *et al*. Nanocomposite bioinks for 3D bioprinting. *Acta Biomater*. 2022;151:45-69.

doi: 10.1016/j.actbio.2022.08.014

31. Hinton TJ, Jallerat Q, Palchesko RN, *et al*. Three-dimensional printing of complex biological structures by freeform reversible embedding of suspended hydrogels. *Sci Adv*. 2015;1(9):e1500758.

doi: 10.1126/sciadv.1500758

32. Sattari S, Mariano CA, Eskandari M. Biaxial mechanical properties of the bronchial tree: Characterization of elasticity, extensibility, and energetics, including the effect of strain rate and preconditioning. *Acta Biomaterialia*. 2023;155:410-422.

doi: 10.1016/j.actbio.2022.10.047

33. Hoffman E, Song Y, Zhang F, *et al*. Regional and disease-specific glycosaminoglycan composition and function in decellularized human lung extracellular matrix. *Acta Biomater*. 2023;168:388-399.

doi: 10.1016/j.actbio.2023.06.043

34. Hoffman ET, Uhl FE, Asarian L, *et al*. Regional and disease specific human lung extracellular matrix composition. *Biomaterials*. 2023;293:121960.

doi: 10.1016/j.biomaterials.2022.121960

35. Uhl FE, Wagner DE, Weiss DJ. Preparation of Decellularized Lung Matrices for Cell Culture and Protein Analysis. *Methods Mol Biol*. 2017;1627:253-283.

doi: 10.1007/978-1-4939-7113-8_18

36. Tashman JW, Shiwarski DJ, Feinberg AW. Development of a high-performance open-source 3D bioprinter. *Sci Rep*. 2022;12(1):22652.

doi: 10.1038/s41598-022-26809-4

37. Tashman JW, Shiwarski DJ, Coffin B, *et al*. In situ volumetric imaging and analysis of FRESH 3D bioprinted constructs using optical coherence tomography. *Biofabrication*. 2022;15(1):014102.

doi: 10.1088/1758-5090/ac975e

38. Bae M, Kim JJ, Kim J, *et al*. Decellularized extracellular matrix for three-dimensional bioprinted in vitro disease modeling. *Int J Bioprint*. 2024;10(2):1970.

doi: 10.36922/ijb.1970

39. Prasad PR, Sahni PK, Mondal D, *et al*. Towards a bioengineered airway: advances in tracheal tissue engineering and biofabrication. *Front Cell Dev Biol*. 2026;14:171343.

doi: 10.3389/fcell.2026.1713743

40. Sirotkina MY, Chabina AS, Lomert EV, *et al*. Effect of Telopeptides in Collagen on the Behavior of Mesenchymal Stromal Cells In Vitro. *Cell and Tissue Biology*. 2024;18(6):699-706.

doi: 10.1134/S1990519X24700603

41. Paglia EB, de Freitas GP, Baldin EKK, *et al*. Innovative approaches in alginate grafting: Amino acids of RGD peptide composition for biomimetic and biocompatible biomaterial. *Int J Biol Macromol*. 2025;322:147080.

doi: 10.1016/j.ijbiomac.2025.147080

42. Wu M, Zhou H, Hu J, *et al*. Decellularized porcine kidney-incorporated hydrogels for cell-laden bioprinting of renal cell carcinoma model. *Int J Bioprint*. 2024;10(1):1413.

doi: 10.36922/ijb.1413

43. Bupesh Raja JK, Y. Díaz G, La Boucan F, *et al*. Advances in decellularized extracellular matrix bioinks for regenerative medicine applications. *Int J Bioprint*. 2025;11(5):23-45.

doi: 10.36922/ijb025210205

44. Brumberg VA, Bikmulina PY, Pozdnyakov AA, *et al*. Scaling liver bioprinting: A guide for usage of the hepatic extracellular matrix as a bioink. *Int J Bioprint*. 2025;11:57-83.

doi: 10.36922/ijb.4343

45. Zhang C, Xu Y, Yu H, *et al*. Fabrication of an in vitro three-dimensional tumor model using liver-derived decellularized extracellular matrix/gelatin methacrylate bioink for investigating cancer characteristics and drug resistance. *Int J Bioprint*. 2025;11(4):025160142.

doi: 10.36922/ijb025160142

46. Li P, Li X, Tang G, *et al*. Emerging frontiers in 3D bioprinting: Harnessing decellularized matrix bioink for advancements in musculoskeletal tissue engineering. *Int J Bioprint*. 2024;10(5):3418.

doi: 10.36922/ijb.3418

47. Polio SR, Kundu AN, Dougan CE, *et al*. Cross-platform mechanical characterization of lung tissue. *PLoS ONE*. 2018;13(10):e0204765.

doi: 10.1371/journal.pone.0204765

48. Elango J, Zamora-Ledezma C. Rheological, Structural, and Biological Trade-Offs in Bioink Design for 3D Bioprinting. *Gels*. 2025:11(8):659.

doi: 10.3390/gels11080659

49. Eskandari M, Arvayo AL, Levenston ME. Mechanical properties of the airway tree: heterogeneous and anisotropic pseudoelastic and viscoelastic tissue responses. *J Appl Physiol*. 2018;125(3):878-888.

doi: 10.1152/japplphysiol.00090.2018

50. Wu Z, Su X, Xu Y, *et al*. Bioprinting three-dimensional cell-laden tissue constructs with controllable degradation. *Sci Rep*. 2016;6(1):24474.

doi: 10.1038/srep24474

51. Tuftee C, Alsberg E, Ozbolat IT, *et al*. Emerging granular hydrogel bioinks to improve biological function in bioprinted constructs. *Trends Biotechnol*. 2024;42(3):339-352.

doi: 10.1016/j.tibtech.2023.09.007

52. Dickenson ME, Oakes RS, Morris AH. Don't judge an implant by its cover: how the foreign body response and fibrotic capsule might be harnessed for good. *npj Biomedical Innovations*. 2026;3(1):3.

doi: 10.1038/s44385-025-00053-7

53. Kenneth Ward W. A review of the foreign-body response to subcutaneously-implanted devices: the role of macrophages and cytokines in biofouling and fibrosis. *J Diabetes Sci Technol*. 2008;2(5):768-777.

doi: 10.1177/193229680800200504

54. Swartzlander MD, Barnes CA, Blakney AK, *et al*. Linking the foreign body response and protein adsorption to PEG-based hydrogels using proteomics. *Biomaterials*. 2015;41:26-36.

doi: 10.1016/j.biomaterials.2014.11.026

55. Appel AA, Ibarra V, Somo SI, *et al*. Imaging of Hydrogel Microsphere Structure and Foreign Body Response Based on Endogenous X-Ray Phase Contrast. *Tissue Eng Part C Methods*. 2016;22(11):1038-1048.

doi: 10.1089/ten.TEC.2016.0253

56. Abraham AA, Means AK, Clubb FJ, Jr., *et al*. Foreign Body Reaction to a Subcutaneously Implanted Self-Cleaning, Thermoresponsive Hydrogel Membrane for Glucose Biosensors. *ACS Biomater Sci Eng*. 2018;4(12):4104-4111.

doi: 10.1021/acsbiomaterials.8b01061

57. Neves MI, Moroni L, Barrias CC. Modulating Alginate Hydrogels for Improved Biological Performance as Cellular 3D Microenvironments. *Front Bioeng Biotechnol*. 2020;8:665.

doi: 10.3389/fbioe.2020.00665

58. Kumar S, Malviya R, Srivastava S, *et al*. Advancements in alginate-derived biomaterials for tissue engineering and regenerative medicine: Emerging innovations and translational outlooks. *J Drug Deliv Sci Technol*. 2025;114:107569.

doi: 10.1016/j.jddst.2025.107569

59. Güven K, Dhawan A, Filippi C. RGD-modified alginate enhances viability, metabolic reprogramming, and cytokine secretion profiles in encapsulated mesenchymal stromal cells. *Sci Rep*. 2026;16(1):14927.

doi: 10.1038/s41598-026-42864-7

60. Cao H, Duan L, Zhang Y, *et al*. Current hydrogel advances in physicochemical and biological response-driven biomedical application diversity. *Signal Transduct Target Ther*. 2021;6(1):426.

doi: 10.1038/s41392-021-00830-x

61. Kim A, Downer MA, Berry CE, *et al*. Investigating Immunomodulatory Biomaterials for Preventing the Foreign Body Response. *Bioengineering*. 2023;10(12):1411.

doi: 10.3390/bioengineering10121411

62. You C, Cao J, Du Y, *et al*. ε-Poly-l-lysine-hydroxyphenyl

propionic acid/IL-4 composite hydrogels with inflammation regulation and antibacterial activity for improving integration stability of soft tissues and orthopedic implants. *Int J Biol Macromol*. 2024;254:127937.

doi: 10.1016/j.ijbiomac.2023.127937

63. Shi C, Pamer EG. Monocyte recruitment during infection and inflammation. *Nat Rev Immunol*. 2011;11(11):762-774.

doi: 10.1038/nri3070

64. Vegas AJ, Veiseh O, Doloff JC, *et al*. Combinatorial hydrogel library enables identification of materials that mitigate the foreign body response in primates. *Nat Biotechnol*. 2016;34(3):345-352.

doi: 10.1038/nbt.3462

65. Hong JY, Seo Y, Davaa G, *et al*. Decellularized brain matrix enhances macrophage polarization and functional improvements in rat spinal cord injury. *Acta Biomater*. 2020;101:357-371.

doi: 10.1016/j.actbio.2019.11.012

66. Ariganello MB, Simionescu DT, Labow RS, *et al*. Macrophage differentiation and polarization on a decellularized pericardial biomaterial. *Biomaterials*. 2011;32(2):439-449.

doi: 10.1016/j.biomaterials.2010.09.004

67. Kasravi M, Ahmadi A, Babajani A, *et al*. Immunogenicity of decellularized extracellular matrix scaffolds: a bottleneck in tissue engineering and regenerative medicine. *Biomater Res*. 2023;27(1):10.

doi: 10.1186/s40824-023-00348-z

68. Butenko S, Nagalla RR, Guerrero-Juarez CF, *et al*. Hydrogel crosslinking modulates macrophages, fibroblasts, and their communication, during wound healing. *Nat Commun*. 2024;15(1):6820.

doi: 10.1038/s41467-024-50072-y

69. De Santis MM, Alsafadi HN, Tas S, *et al*. Extracellular-Matrix-Reinforced Bioinks for 3D Bioprinting Human Tissue. *Adv Mater*. 2021;33(3):2005476.

doi: 10.1002/adma.202005476

70. Liang Y, Wei S, Zhang A. Bioengineered tracheal graft with enhanced vascularization and mechanical stability for functional airway reconstruction. *Regen Ther*. 2025;29:364-380.

doi: 10.1016/j.reth.2025.03.016

71. Yeou SH, Shin YS. Tissue-Engineered Tracheal Reconstruction. *Biomimetics*. 2025;10(7):457.

doi: 10.3390/biomimetics10070457

72. Fonseca KB, Gomes DB, Lee K, *et al*. Injectable MMP-sensitive alginate hydrogels as hMSC delivery systems. *Biomacromolecules*. 2014;15(1):380-390.

doi: 10.1021/bm4016495